The Wettzell–Onsala G130128 Experiment
– VLBI Observations of a GLONASS Satellite –

Rüdiger Haas[1], Alexander Neidhardt[2], Jan Kodet[2], Christian Plötz[3], Ulrich Schreiber[2], Gerhard Kronschnabl[3], Sergei Pogrebenko[4], Dmitry Duev[4], Simon Casey[1], Ivan Marti-Vidal[1], Jun Yang[1], Lucia Plank[5]

Abstract We describe the Wettzell-Onsala G130128 experiment, where for the first time a GLONASS satellite was observed in VLBI mode with the new L-band system on the 20-m radio telescope in Wettzell. Fringes were successfully found using two independent software correlators and three independent a priori delay models. The RMS scatter of the derived phase delays is below 10 ps for solution intervals of 2 s and larger. The RMS scatter of the derived group delays is below 1.5 ns for solution intervals of 30 s and larger. The total delays, using the three different a priori delay models, agree on the level of 0.8–0.9 ns and 0.2–0.4 ns, for groups delays and integrated delay rates, respectively.

Keywords GNSS-VLBI, GLONASS, a priori delay models, SFXC, DiFX

1 Introduction

During recent years the topic of an improved connection of the VLBI and GNSS reference frames has been discussed. Currently, these techniques are linked together at ground-based co-location stations only. This kind of connection relies on local surveys at the sites to be able to link the reference points of the different instruments used for geodetic VLBI observations and GNSS observations, respectively. To improve the connection of the techniques, the idea of observing GNSS satellites with VLBI has been brought up, e.g. [1, 2]. Several such GNSS-VLBI experiments have been performed during recent years, where a stochastic delay measurement noise of 80 ps in 1 s and 4 ps in 15 min could be achieved [2]. Because GNSS signals are in the L-band, radio telescopes with L-band receivers are needed for such observations. However, geodetic radio telescopes are usually only equipped with S/X-band receivers. Thus these telescopes cannot be used for GNSS-VLBI experiments. To overcome this restriction, an L-band system that extracts the L-band signal from the S-band signal chain has been developed at Wettzell [3, 4]. To test this new instrumentation, a test experiment was conducted in early 2013.

1. Chalmers University of Technology (Sweden)
2. Technische Universität München (Germany)
3. Federal Agency for Cartography and Geodesy (Germany)
4. Joint Institute for VLBI in Europe (The Netherlands)
5. University of Tasmania (Australia)

2 The Observations

The G130128 experiment was conducted on January 28, 2013, on the Onsala–Wettzell baseline. At Onsala, the 25-m telescope with an L-band receiver was used, while at Wettzell, the 20-m telescope with the specially developed L-band receiver was utilized. The observations concentrated on one GLONASS satellite (Norad # 37139, GLONASS-736, PR09), that was observed for 45 minutes, in nine scans of four minutes length each and one minute breaks. Four IF channels of 8 MHz bandwidth were observed with the central frequency at 1586.87 MHz. The observing plan was prepared by JIVE (Joint Institute for VLBI in Europe) and included a stop-and-go tracking of the satellite with 15 second updates. Because the primary goal was to test the L-band receiver at Wettzell, no calibrator source was observed.

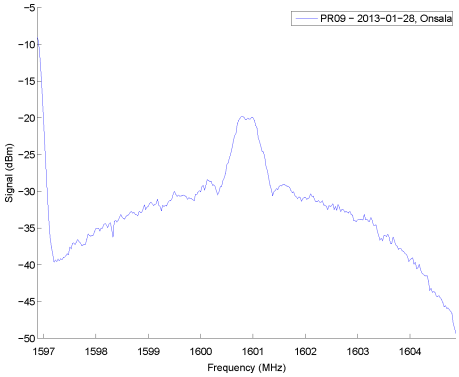

Fig. 1 Signal spectrum of PR09 (Norad # 37139, GLONASS-736) observed on 2013-01-28 at Onsala.

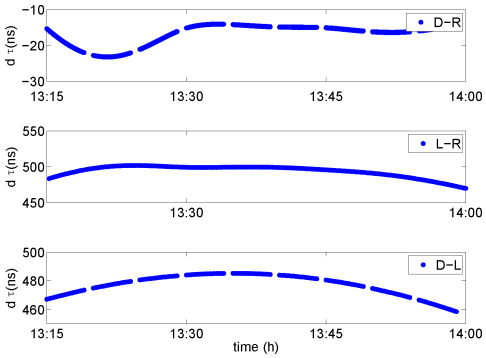

Fig. 2 Comparison of a priori delay values. Shown are the differences between the D- and R-model (top), L- and R-model (middle), and D- and L-model (bottom).

As the Onsala 25-m telescope is equipped with a dedicated L-band receiving system, the satellite signal strength had to be attenuated in the RF regime by 30 dB, in order to avoid saturation. A picture of the resulting signal spectrum is presented in Figure 1 and clearly shows the GLONASS signal.

On the other hand, the L-band signal at Wettzell is extracted via the S-band horn that is attenuating the L-Band frequencies by about 60 dB. Thus, here the signal had to be amplified by 30 dB before the receiver. The spectrum of the signal was not visible at the station.

3 A priori Delay Modeling and Data Correlation

A priori delay values were modeled with three different approaches. The first set of a priori delays was calculated by Dmitry Duev as described in [5]. These values included the geometrical, ionospheric, and tropospheric contributions, as well as the axis offset at the Onsala 25-m telescope. In the following discussion, these a priori delay values are referred to as D-model.

The second set of a priori delay values was calculated by Lucia Plank [6], following [7]. These values included only the geometrical contributions and will be referred to as L-model in the following discussion.

The last set of a priori delays were calculated by Rüdiger Haas following [8] and also only included the geometrical contributions. The satellite positions for these calculations were based on final ephemerides with 15 min temporal resolution provided by CODE (Center for Orbit Determination in Europe). These a priori values will be referred to as R-model.

Figure 2 depicts a comparison of the geometrical part of the three sets of a priori delays. The D- and R- model, both calculating geocentric delays, agree on the level of about 15 ns. Probably, part of the detected differences is due to different treatment of the a priori satellite orbit information and necessary interpolation between satellite positions that are only given at discrete epochs. The differences between the L-model and the other two models are larger and on the order of about 490 ns. This rather large difference is due to the L-delays being topocentric.

4 Preliminary Analysis

The correlation of the observed data was done with two different software correlators, the SFXC [9] at the Joint Institute for VLBI in Europe (JIVE) and the DiFX [10], installed at the Onsala Space Observatory. The SFXC correlation explicitly used the a priori delays of the D-model, while the DiFX correlation was done with all three sets of a priori delays.

As an example, the amplitudes and phases, as derived from the correlation with DiFX using the D-model, are presented in Figure 3. The DiFX correlation was done with 0.25 s integration time, and the figure depicts the average of the nine scans of four minutes length each. In all four IF channels, a rapid phase change is clearly visible, and clear and strong amplitudes are detected.

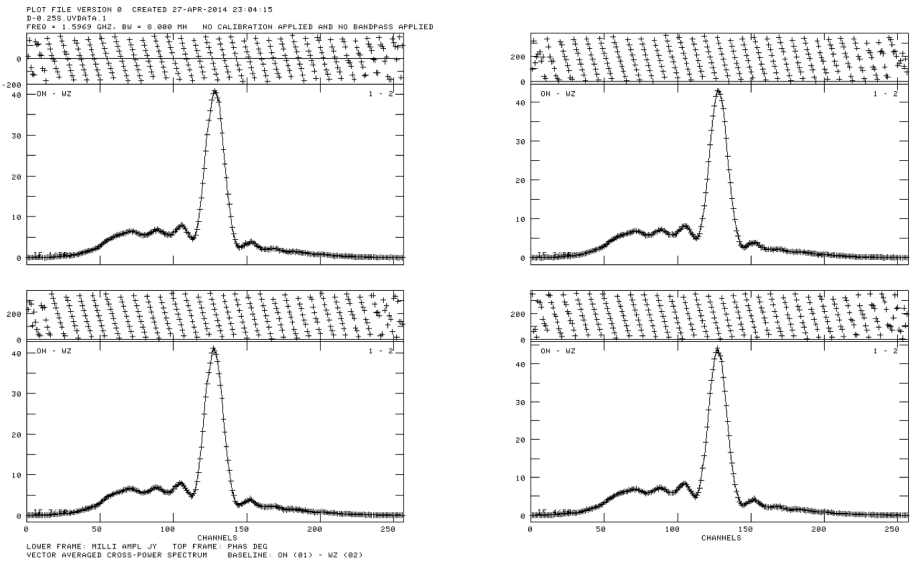

Fig. 3 Amplitudes and phases in the four IF channels after correlation with DiFX using the a priori delay values of the D-model.

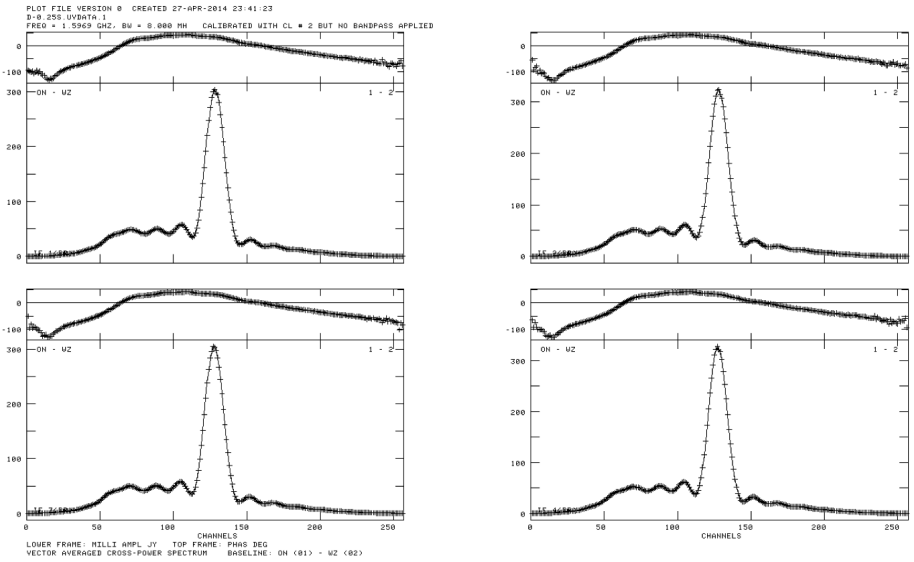

Fig. 4 Amplitudes and phases in the four IF channels after fringe-fitting with AIPS [11] with a 30 s solution interval.

Fringe-fitting with AIPS [11] was done for 0.25 s, 1 s, 2 s, and 30 s solution intervals. Figure 4 depicts the corresponding amplitudes and phases after fringe-fitting with a 0.25 s solution interval. The phases in the four IFs are now stable. The remaining non-flat phase residual and the amplitude bandpass shape are due to the instrument response and can be calibrated in future observations.

After fringe-fitting with AIPS, group delays, delay rates, and phases were compared for the three correlations. Figure 5 depicts the raw phases after fringe-fitting with a 30 s solution interval. For the correlation using the D-model, the raw phases (black triangles in Figure 5) could be unwrapped without problems, and phase delays could easily be determined. However, for the correlations with the L- and R-models, some problems occurred with phase unwrapping. This indicates

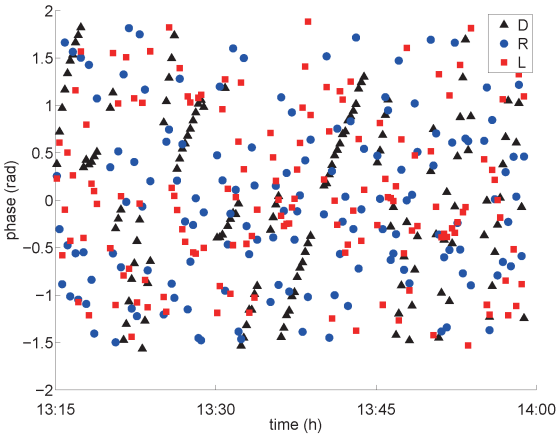

Fig. 5 Raw phases after fringe-fitting with AIPS with a 30 s solution interval. The phases need to be unwrapped before phase delays can be obtained. The unwrapping worked fine for values from the correlation with the D-model (black triangles), but failed for the other two (R-model, blue circles; L-model, red squares) where not all phase ambiguities could be resolved.

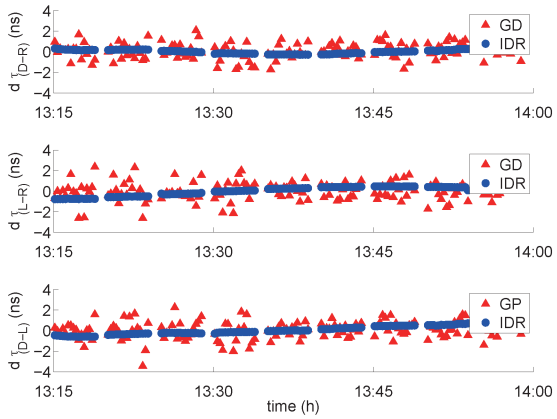

Fig. 7 Comparison of total delays, i.e., a priori delays plus residual delays from the the DiFX correlation and post-processing. Shown are the differences between processing with the D- and R-model (top), L- and R-model (middle), and D- and L-model (bottom). Results based on group delays (GD) are shown as red triangles, based on integrated delay rates (IDR) as blue circles.

that improvements are still necessary for these two a priori models.

For all three correlation sets, the delay rates could be integrated. As an example, Figure 6 depicts the group delays, integrated delay rates, and phase delays of the DiFX correlation using the D-model and subsequent fringe-fitting with AIPS with a 30 s solution interval. It is clearly visible that the group delays have a much larger scatter than both the integrated delay rates and the phase delays. Table 1 presents the RMS scatter for different solution intervals. Already for a solution interval of 2 s, phase delays and integrated delay rates reach an RMS scatter level of about 10 ps, while group delays do not reach an RMS scatter below 1.5 ns before a solution interval of 30 s.

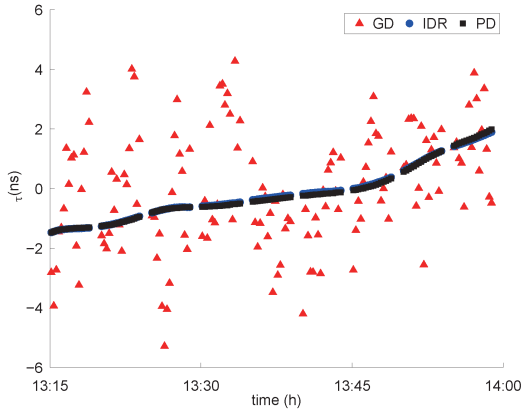

Fig. 6 Group delay (red triangles), integrated delay rate (blue circles), and phase delay (black squares) results from the DiFX correlation using a priori delay values of the D-model.

Table 1 RMS scatter after fringe-fitting with different solution intervals. The correlation itself was done using a priori delay values according to the D-model and the DiFX software correlator.

Solution interval	RMS scatter		
	group delays	integrated delay rates	phase delays
1 s	5.9 ns	17.6 ps	12.5 ps
2 s	3.9 ns	9.5 ps	8.7 ps
30 s	1.4 ns	9.1 ps	8.8 ps

The fringe-fitted delay residuals from AIPS were added to the corresponding a priori delay models to give total delays. The differences for the total delays for the three models are presented in Figure 7, and the corresponding RMS scatter of these differences are given in Table 2. The agreement is on a level of 0.8–0.9 ns for group delays and 0.2–0.4 ns for phase delays (approximated by integrated delay rates).

5 Conclusions and Outlook

The G130128 experiment verifies that the L-band system on the Wettzell 20-m radio telescope, which is

Table 2 RMS scatter of the total delay differences between the three different correlations using the three different a priori delay models, the D-, R- and L-model.

Difference	RMS group delays	RMS integrated delay rates
D–R	0.76 ns	0.22 ns
L–R	0.88 ns	0.22 ns
D–L	0.86 ns	0.42 ns

regularly used for geodetic VLBI, works fine. Fringes were successfully found on the Wettzell-Onsala baseline with two independent software correlators, SFXC and DiFX. For the DiFX correlations, three different and independent a priori delay models were used, and fringes were found with all three approaches. The correlation results were post-processed with AIPS. For the correlation using the D-model, group delays, integrated delay rates, and phase delays could be determined successfully. For correlations using the two other a priori models, group delays and integrated delay rates could be determined, but the phase delay determination suffered from unresolved phase ambiguities.

The RMS scatter of the phase delays was on the level of 10 ps for solution intervals of 2 s, while group delays reached an RMS scatter below 1.5 ns for solution intervals not shorter than 30 s.

Total delay values, i.e., a priori delay models plus fringe-fitted delay residuals from AIPS, agreed on a level of 0.8–0.9 ns for group delays and 0.2–0.4 ns for phase delays (approximated by integrated delay rates) between the three different correlations. This indicates that the L- and R-model for a priori delay values need to be improved, which was also evident from the unresolved ambiguities for the phase delay determination.

For the future, we are planning improvements of post-processing by, e.g., bandpass calibration and doppler tracking to remove time-dependent phase residual errors. We are also planning further experiments to observe GLONASS satellites with VLBI, involving more VLBI stations and observing several GLONASS satellites, which shall also be simultaneously observed with satellite laser ranging (SLR). Furthermore, we plan for a dedicated L/S/X session involving the 20-m radio telescope at Wettzell, which is able to receive all three frequency bands, and the two radio telescopes at Onsala, the 25-m telescope with L-band capability, and the 20-m telescope with S/X capability. This approach will allow us to observe geodetic radio sources with the S/X systems and GLONASS satellites with the L-band systems in the same experiment.

References

1. Tornatore V., Haas R., Duev D., Pogrebenko S., Casey S., Molera Calvés G., Keimpema A. Single baseline GLONASS observations with VLBI: data processing and first results. *Proc. 20th European VLBI for Geodesy and Astrometry Working Meeting*, 162–165, 2011.
2. Tornatore V., Haas R., Duev D., Pogrebenko S., Casey S., Molera Calvés G. Direct VLBI Observations of Global Navigation Satellite System Signals. *Proc. of the IAG General Assembly 2011*, International Association of Geodesy Symposia Volume 139, Eds.C. Rizo & P. Willis, 247–252, 2014. doi:10.1007/978-3-642-37222-3_32
3. Kodet J., Plötz Ch., Schreiber K. U., Neidhardt A., Pogrebenko S., Haas R., Molera Calvés G., Prochazka I. Colocation of space geodetics techniques in space and on the ground. *Proc. 21st European VLBI Group for Geodesy and Astronomy Working Meeting*, Eds. N. Zubko & M. Poutanen, 2013:1, 223–226, 2013.
4. Kodet J., Schreiber K. U., Plötz Ch., Neidhardt A., Kronschnabl G., Haas R., Molera Calvés G., Pogrebenko S., Rothacher M., Maennel B., Plank L., Hellerschmied A. Colocations of Space Geodetic Techniques on Ground and in Space. *IVS 2014 General Meeting Proceedings*, 2014, this volume.
5. Duev D. A., Molera Calvés G., Pogrebenko S. V., Gurvits L. I., Cimó G., Bocanegra Bahamon T. Spacecraft VLBI and Doppler tracking: algorithms and implementation. *Astronomy & Astrophysics*, 541, A43, 2012. doi:10.1051/0004-6361/201218885
6. Plank L. VLBI satellite tracking for the realization of frame ties. *Veröffentlichungen des Departments für Geodäsie und Geoinformation*, Vienna University of Technology, Geowissenschaftliche Mitteilungen, Nr. 95, 2014.
7. Klioner S. A. General Relativistic Model of VLBI Observables. In: *Proc. AGU Chapman Conference on Geodetic VLBI: Monitoring Global Change*, 188–202, NOAA Technical Report 137, NGS 49, 1991.
8. Moyer T. D. Formulation for Observed and Computed Values of Deep Space Network Data Types for Navigation. *Deep Space Communications and Navigation Series, Monograph 2*, JPL Publication 00-7. Jet Propulsion Laboratory, California Institute of Technology, 2000.
9. Keimpema K. A., Duev D. A., Pogrebenko S. V., et al. Spacecraft tracking with the SFXC software correlator. In: *URSI-BeNeLux 2011*, ESTEC, The Netherlands, 2011.
10. Deller A. T., Tingay S. J., Bailes M., West C. DiFX: A Software Correlator for Very Long Baseline Interferometry Using Multiprocessor Computing Environments. *The Publications of the Astronomical Society of the Pacific*, Volume 119, Issue 853, 318–336, 2007.
11. http://www.aips.nrao.edu/index.shtml